How to cite: *Angew. Chem. Int. Ed.* **2024**, *63*, e202401421
doi.org/10.1002/anie.202401421

Main-Group Chemistry

$Cr_{5.7}Si_{2.3}P_8N_{24}$ – A Chromium(+IV) Nitridosilicate Phosphate with Amphibole-Type Structure

Monika M. Pointner, Katherine R. Fisher, Martin Weidemann, Florian Wolf, Jonathan P. Wright, Eleanor Lawrence Bright, Carlotta Giacobbe, Oliver Oeckler, and Wolfgang Schnick**

Abstract: The first nitridic analog of an amphibole mineral, the quaternary nitridosilicate phosphate $Cr_{5.7}Si_{2.3}P_8N_{24}$ was synthesized under high-pressure high-temperature conditions at 1400 °C and 12 GPa from the binary nitrides Cr_2N, Si_3N_4 and P_3N_5, using NH_4N_3 and NH_4F as additional nitrogen source and mineralizing agent, respectively. The crystal structure was elucidated by single-crystal X-ray diffraction with microfocused synchrotron radiation (*C*2/*m*, $a = 9.6002(19)$, $b = 17.107(3)$, $c = 4.8530(10)$ Å, $\beta = 109.65(3)°$). The elemental composition was analyzed by energy dispersive X-ray spectroscopy. The structure consists of vertex-sharing PN_4-tetrahedra forming *zweier* double chains and edge-sharing (Si,Cr)-centered octahedra forming separated ribbons. Atomic resolution scanning transmission electron microscopy shows ordered Si and Cr sites next to a disordered Si/Cr site. Optical spectroscopy indicates a band gap of 2.1 eV. Susceptibility measurements show paramagnetic behavior and support the oxidation state Cr^{+IV}, which is confirmed by EPR. The comprehensive analysis expands the field of Cr–N chemistry and provides access to a nitride analog of one of the most prevalent silicate structures.

Silicates are known for their extensive structural diversity that ranges from individual SiO_4-tetrahedra, over chains and sheets to complex network structures. The abundance of Si and O in terms of total mass is the reason why the group of silicates constitutes the majority of the earth's crust but beyond that, the reason why silicates are the mineral group with the most known number of phases is the adaptability of SiO_4-tetrahedra to form various condensation patters.[1] The family of silicates includes amphibole minerals, whose name, first given by René J. Haüy in 1801, aims for their diversity in composition and appearance. Like all silicate minerals, the basic building blocks are silicate tetrahedra, which here are condensed into $[Si_4O_{11}]^{6-}$ double chains. Their microscopic and macroscopic properties originate from the atomic arrangement often resulting in a fiber-like structure. The main characteristic properties of these fibers are chemical inertia and thermal, electrical and sound insulation, leading to several industrial products that include insulation materials for construction, as well as brake linings and pads. Throughout most of the 20th century, amphiboles were commonly used worldwide as a building material and manufactured into approximately 3,000 products by the 1960s and the estimated consumption still stood at roughly $2 \cdot 10^6$ tons in 2010.[2]

Nitridophosphates have attracted significant interest due to the isoelectronic relation of Si/O and P/N. Nitridophosphate structures are often related to those of silicates resulting in similar motifs, primarily based on PN_4-tetrahedra. The close relation between silicates and nitridophosphates becomes most evident in structures that do not only contain the same motifs but feature the same topology. The recently discovered mica and paracelsian counterparts $AESi_3P_4N_{10}(NH)_2$ (*AE*=Mg, Ca, Sr) and $LiNdP_4N_8$, respectively, represent such close analogs.[3–4] Reactions under high-pressure high-temperature (HP/HT) conditions made their discovery possible, however, the synthesis of nitridophosphates has to overcome some challenges. Their formation is unfavorable in the presence of oxygen due to the

[*] M.Sc. M. M. Pointner, M.Sc. M. Weidemann, M.Sc. F. Wolf, Prof. Dr. W. Schnick
Department of Chemistry
Ludwig-Maximilians-University Munich
Butenandtstraße 5–13, 81377 Munich, Germany
E-mail: wolfgang.schnick@uni-muenchen.de

Dr. K. R. Fisher
Department of Chemical and Pharmaceutical Sciences
London Metropolitan University
166-220 Holloway Road, London N7 8DB, United Kingdom

Dr. J. P. Wright, Dr. E. L. Bright, Dr. C. Giacobbe
ESRF, The European Synchrotron
71 Avenue des Martyrs, CS40220, 38043 Grenoble Cedex 9, France

Prof. Dr. O. Oeckler
Institute of Inorganic Chemistry and Crystallography
Leipzig University
Scharnhorststraße 20, 04275 Leipzig, Germany
E-mail: oliver.oeckler@gmx.de

preferred formation of oxides. A key precursor for most nitridophosphate syntheses is P_3N_5, which has a decomposition temperature of 850 °C. Yet, many easily accessible binary nitrides are inert up to higher temperatures. Further complications include the reduction of P^{+V} to lower oxidation states and the favored formation of stable metal phosphides. This becomes especially prominent in the synthesis of transition metal (*TM*) nitridophosphates with higher oxidation states of the *TM*. A HP/HT approach has successfully addressed these challenges. Furthermore, the utilization of mineralizers has made compound classes accessible that were previously unattainable even by HP/HT conditions. NH_4F-mediated synthesis may exploit the fluorophily of Si as known from industrial processes of etching with HF. This strategy, performed at pressures in the GPa range and temperatures exceeding 1000 °C provides thermal energy for reactions of P_3N_5 with Si_3N_4 or stable refractory *TM* nitrides. This synthetic pathway not only yielded the above mentioned mica analogs but resulted in the formation of mixed nitridosilicate phosphates and *TM* nitridophosphates.[3,5–6]

Herein, we report on $Cr_{5.7}Si_{2.3}P_8N_{24}$, the first amphibole-type nitridophosphate. Following the mineralizer-assisted HP/HT approach, the title compound is accessible at 12 GPa and 1400 °C starting from the respective binary nitrides Cr_2N, Si_3N_4, and P_3N_5, with NH_4F added as a mineralizing agent and NH_4N_3 employed as an additional nitrogen source. The synthesis, described by equation (1), involves the oxidation of chromium and the reduction of nitrogen. A modified Walker-type multianvil module was used, and further details on the synthesis are given in the Supporting Information.

$$2.85\ Cr_2N + 2.67\ P_3N_5 + 0.77\ Si_3N_4 + 1.8\ NH_4N_3 \rightarrow Cr_{5.7}Si_{2.3}P_8N_{24} + 2.4\ NH_3 \quad (1)$$

The reaction yields a red-brown microcrystalline powder, which is stable toward air and moisture at ambient conditions. Crystallites exhibit an intergrown fiber-like morphology with a length of up to at least 7 μm and a width of up to 2 μm that makes single-crystal analysis challenging (Figure 1, left). Pre-characterization of crystallites by transmission electron microscopy (TEM) made it possible to obtain single-crystal data. Crystals of around 2 to 3 μm in size (Figure 1, right) were identified on TEM grids by energy dispersive X-ray (EDX) spectroscopy and selected area electron diffraction (SAED). The precise position was recorded (Figure S1), and single-crystal X-ray diffraction (SCXRD) data were collected using a microfocused synchrotron beam at beamline ID11 of the ESRF (Grenoble, France). The crystal structure of $Cr_{5.7}Si_{2.3}P_8N_{24}$ was solved and refined in the monoclinic space group *C*2/*m* (no. 12, $a=9.6002(19)$, $b=17.107(3)$, $c=4.8530(10)$ Å, $\beta=109.65(3)°$, $Z=2$, $R_1=0.0255$; more details can be found in the Supporting Information). A tilt series of SAED patterns matches simulations and thus confirms the unit cell metrics in space group *C*2/*m* (Figure S2). Based on the structure model from SCXRD, the product was identified as the main constituent by Rietveld refinement (Figure S3) on powder data. High-temperature powder XRD data of $Cr_{5.7}Si_{2.3}P_8N_{24}$ demonstrate stability up to at least 900 °C in air and show a minor thermal expansion up until 900 °C of <8 % (Figure S4). The elemental composition was analyzed by scanning (transmission) electron microscopy (SEM/STEM) EDX; the results fit well with respect to the atomic ratio of Cr : Si : P of 2.85 : 1 : 4 (Table S6). EDX measurements and a FTIR spectrum (Figure S5) indicate a minor amount of oxygen in the compound and a slight sensitivity to moisture or minor compositional variations cannot be ruled out.

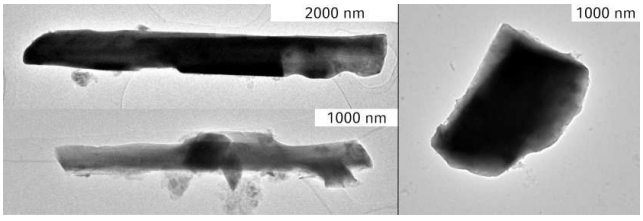

Figure 1. Exemplary TEM bright-field images of crystallites of $Cr_{5.7}Si_{2.3}P_8N_{24}$ (left), crystallite used for data collection at beamline ID11 with microfocused synchrotron beam (right).

Crystal structures of amphiboles can adopt monoclinic (clinoamphiboles) or orthorhombic (orthoamphiboles) structures with clinoamphiboles in the space group *C*2/*m* exhibiting the widest range of compositions and cell dimensions. $Cr_{5.7}Si_{2.3}P_8N_{24}$ adopts *C*2/*m* and shows a pronounced structural distortion with the largest β (109.65(3)°) reported for any clinoamphibole. The structure consists of a rigid framework with two principal elements—*zweier* (as defined by Liebau[1]) double chains of vertex-sharing PN_4-tetrahedra and ribbons of edge-sharing octahedra. A unit cell with partially denoted atom sites is displayed in Figure 2a.

The unbranched *zweier* double chains ($[P_4N_{11}]^{13-}$) contain two crystallographically distinct tetrahedra centers, that alternate along the double chain. Both are occupied by P. Interatomic P–N distances range from 1.6026(11) to 1.6574 (11) Å and are comparable to those in compounds like TiP_4N_8 (1.5758(15)–1.645(3) Å), $Sc_5P_{12}N_{23}O_3$ (1.5720(10)–1.6434(10) Å) and $AlP_6O_{3x}(NH)_{3-3x}N_9$ with $x\approx0.33$ (1.602(3)–1.6585(15) Å).[5,7–8] The structure contains five crystallographically independent octahedrally coordinated sites. Four out of the five form ribbons that extend along *c*. Figure 2b shows the ribbons and their offset to each other by half a unit cell along both *a* and *b*. Cr5 is isolated from other octahedra and only shares vertices with tetrahedra. This site is commonly vacant or occupied by large, low-in-charge alkali metals and often shows a high degree of positional disorder. All coordination polyhedra are illustrated in Figure S6. In naturally occurring amphiboles, these octahedral sites are traditionally classified as cation positions A, B, and C with the defined crystallographic sites *M*(1), *M*(2), *M*(3) [C], *M*(4) [B] and *A* [A]. Different atoms with varying sizes and charges occupy these cation positions. However, in $Cr_{5.7}Si_{2.3}P_8N_{24}$, the occupation by Cr^{+IV} and Si^{+IV} (55 and 40 pm ionic radius, CN = 6, respectively) does not follow this concept of separation.[9] Refinement of Si and

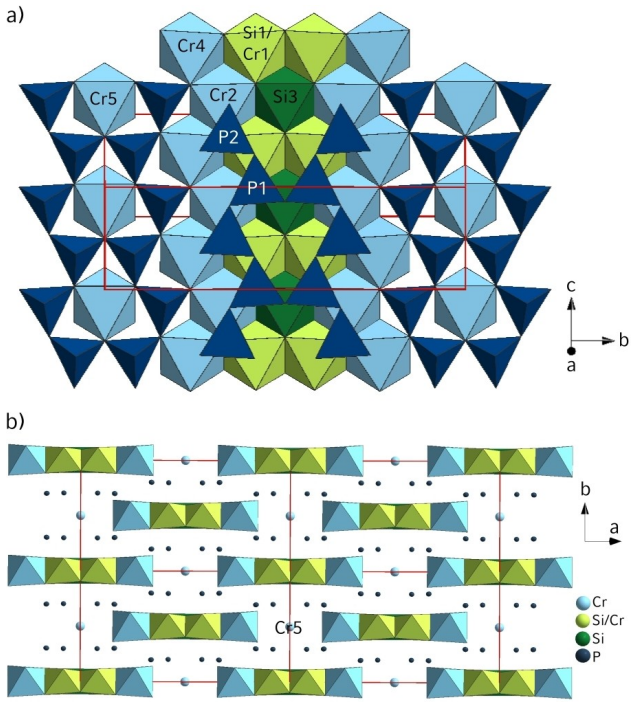

Figure 2. **a)** The crystal structure of $Cr_{5.7}Si_{2.3}P_8N_{24}$ consists of a three-dimensional rigid framework with *zweier* double chains of vertex-sharing PN_4-tetrahedra and ribbons of edge-sharing CrN_6- (light blue), $(Cr_{0.3}Si_{0.7})N_6$- (light green) and SiN_6- (dark green) octahedra. The octahedral Cr5 (light blue) site is isolated from other octahedra. Polyhedra are partially denoted. The unit cell is outlined in red; **b)** Ribbons of edge-sharing octahedra are displayed in four unit cells that shows their offset from each other by half a unit cell along both *a* and *b*. Isolated $Cr5N_6$-octahedra are positioned in between.

Cr positional parameters resulted in a structure model with one occupationally disordered site of 0.7:0.3 of Si^{+IV} and Cr^{+IV} (Si1/Cr1). This could be affirmed by comparison of bond lengths and octahedra volumes as the disordered position displays only a slight deviation of 2% from the expected values of a 0.7:0.3 Si:Cr mixed occupancy (Table S7). STEM high-angle annular dark field (HAADF) images with a Z contrast proportional to Z^2 ($Z_{Cr}=24$, $Z_{Si}=14$) show different cation-site occupations fitting to fully occupied Cr, fully occupied Si and an occupational disorder on Si1/Cr1 on the expected positions (Figure 3 left).[10] The Cr5 site exhibits a lower site symmetry (2/*m*) compared to other Cr sites (2) and therefore a halved absolute intensity compared to the position Cr2.

The tetrahedra double chain in $Cr_{5.7}Si_{2.3}P_8N_{24}$ has a smaller repeat distance (4.85510(11) Å) compared to naturally occurring amphiboles like α-grunerite ($Fe_{5.26}Mg_{1.67}Ca_{0.05}Si_8O_{22}(OH)_2$, 5.3382(9) Å).[11] The presence of P in the tetrahedral position, replacing Si (ionic radius: P = 17 pm, Si = 26 pm), contributes to the reduction in tetrahedra size and the double-chain repeat distance.[9] The reverse effect is observed whenever Al (ionic radius 39 pm) occupies tetrahedral sites.[9,12] The kinking angle N5–N6–N5 serves as a parameter to quantify the structural distortion. $Cr_{5.7}Si_{2.3}P_8N_{24}$ exhibits a kinking angle of 127.78(7)°, surpassing the high-pressure polymorph of grunerite (137.5(4)°, γ-phase *C*2/*m*, 22 GPa), which had the lowest reported kinking angle so far found in an amphibole, indicating significant structural distortion of the double chain (Figure S7).[10]

Partial values of the Madelung part of lattice energy were compared with literature values to review the electrostatic plausibility of the structure model and provided a sufficient level of agreement (Table S8). Bond valence sums (BVS) show a notable deviation for the Cr5 site, a phenomenon that can also be observed in other amphiboles for the respective site (Table S8–S9). This is most likely due to the disorder on this position, which leads to pronounced bond length variations. BVS calculations support the assignment of Si und P to octahedral and tetrahedral sites, respectively. Since a definite assignment of Si and P from X-

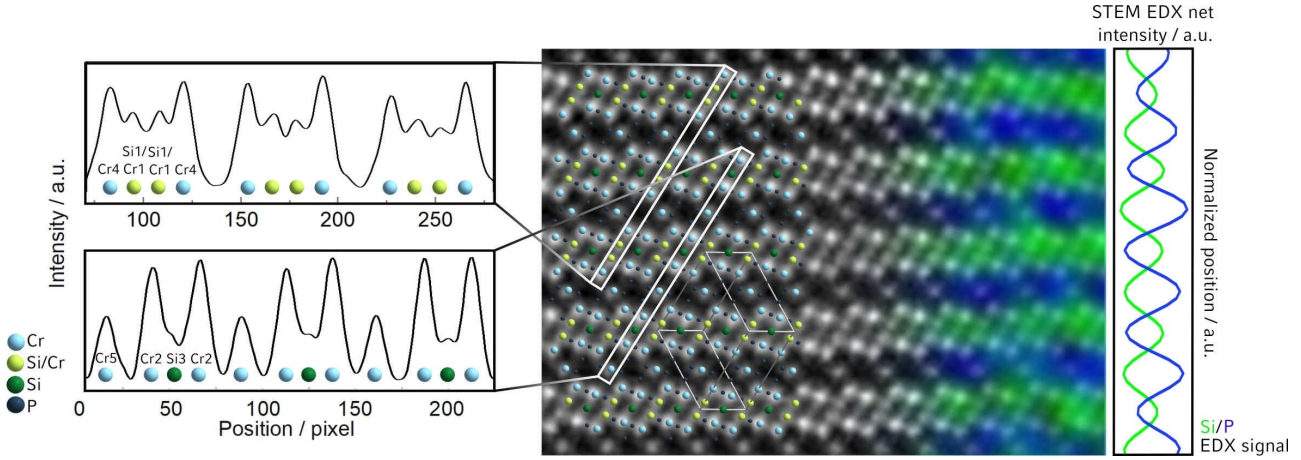

Figure 3. STEM-HAADF image (middle) of $Cr_{5.7}Si_{2.3}P_8N_{24}$ along [112] with structure overlay: Cr light blue, Si dark green, Si/Cr disorder light green, P dark blue. Intensity profiles (left) demonstrate the difference in intensity corresponding to different occupancies of atom columns by Cr, Si/Cr and Si atoms. Isolated Cr5 site exhibits a lower site symmetry (2/m) compared to other Cr sites (2) and therefore a lower absolute intensity. STEM-EDX map as overlay (right) shows separated intensity maxima for the EDX signal of P (blue) and Si (green). Unit cell is shown in light gray. An enlarged version of the STEM-HAADF image is given in Figure S8.

ray data is not possible given the similar X-ray scattering form factors, STEM-EDX mapping was performed. An overlay with an HAADF image (Figure 3, right) suggests ordering of Si and P that leads to the conclusion that the title compound consists of PN_4-tetrahedra and SiN_6-octahedra. In nitrides, the high-pressure motif of sixfold N-coordinated Si has so far only been observed in cubic γ-Si_3N_4, and the two nitride imides $SiP_2N_4(NH)$ and $AESi_3P_4N_{10}(NH)_2$ (*AE*=Mg, Ca, Sr).[3,13–14]

Magnetic measurements of 3*d* transition metals are sensitive to oxidation states. Especially in compounds with a metallic character, e.g., compounds with an antiperovskite structure type and the general formula Cr_3MN, an assignment of oxidation states is not easily possible.[15–18] Many structures feature Cr^{+III}, such as CrN and (Cr,*M*)N solid solutions, as well as nitridochromates like AE_3CrN_3.[19–23] So far, the number of known nitridic compounds with chromium(+IV) is very limited and examples include the electride $Sr_3CrN_3:e^-$ and $LiSr_2[CrN_3]$.[24–25] Oxidation states higher than +IV range up to the maximum of +VI.[26–31] A comprehensive list providing an overview of known binary, ternary and quaternary chromium nitrides and nitridochromates can be found in Table S10. The magnetic susceptibility was measured between 1.9 and 300 K at a constant field of 3 T (Figure 4a). The open-shell configuration of Cr^{+IV} with two unpaired electrons (d^2, electron configuration [Ar]$3d^2 4s^0$) is responsible for the magnetic properties of $Cr_{5.7}Si_{2.3}P_8N_{24}$. Results show paramagnetic behavior down to low temperatures with an effective magnetic moment of $\mu_{eff}=2.473(2)\,\mu_B$ per formula unit obtained from a Curie–Weiss fit of the inverse molar susceptibility (inset in Figure 4a). This is in agreement with comparable literature data and the theoretical value of $\mu_{eff}=2.83\,\mu_B$ for an electronic ground state $^3T_{1g}$ in a d^2 system following the spin-only formula.[32] Magnetization isotherm and zero-field-cooled/field-cooled magnetization data indicate minor impurities by an unknown ferromagnetic and diamagnetic substance (Figures S10–S11), which are highly unlikely to be CrP, as CrP also exhibits Pauli paramagnetism.[33] The electron paramagnetic resonance (EPR) spectrum has a sharp central feature with a turning point at about 35 mT without significant secondary side features (Figure 4b). Simulations for Cr^{+III} and Cr^{+IV} for all four Cr positions are calculated, and Cr^{+IV} shows by far the best-fitting results. The simulation for Cr^{+III} and further information are given in Figure S12 and Table S11. The magnetic measurements support the conclusion that exclusively Cr^{+IV} is present in the title compound.

The optical band gap of $Cr_{5.7}Si_{2.3}P_8N_{24}$ can be approximated from the valence to conduction band transition visible in the UV/Vis-spectrum by converting reflectance spectra to the Kubelka–Munk function and calculating a Tauc plot (Figures 4c, S13). The estimated direct band gap of 2.1 eV indicates that $Cr_{5.7}Si_{2.3}P_8N_{24}$ is a semiconducting material. Nitride semiconductors with layered structures such as delafossite-type $CuNbN_2$ and $CuTaN_2$ feature a strong optical absorption onset at 1.4–1.5 eV.[34–35] Other nitride semiconductors with band gaps in a similar region are $ZnSnN_2$ (1–2 eV) with a strong dependence on the degree of cation disorder, Ta_3N_5 (1.8–1.9 eV) and InN thin films (1.5–2.5 eV).[36–39]

Summing up, we present the first nitridic analog of an amphibole mineral. $Cr_{5.7}Si_{2.3}P_8N_{24}$ was obtained by a NH_4F-mediated HP/HT synthesis. Separated Si and P sites, as well as a disordered Si:Cr site could be validated by STEM-HAADF analysis. The oxidation state of Cr is +IV and even though $Cr^{+IV}O_2$ has been a key magnetic storage material dominating data storage in high-performance audio tapes for years, Cr^{+IV} has only been scarcely observed in nitrides prior to this work. The chemical diversity of amphiboles becomes evident by the array of used prefixes, different sized cation positions and frequent anion substitution. We expect that further research on complete and partial substitution of the cation positions by other transition metal and alkali metal ions can provide access to stable nitrides with interesting physical properties like suitable band gaps for semiconductor applications and ion conductivity. This seems close as chromium containing nitrides and transition metal nitrides in general are already being investigated as co-catalyst for photocatalytic hydrogen production or as materials for novel energy harvesting and Fe-rich amphiboles exhibit electric conductivity.[40–44] Fur-

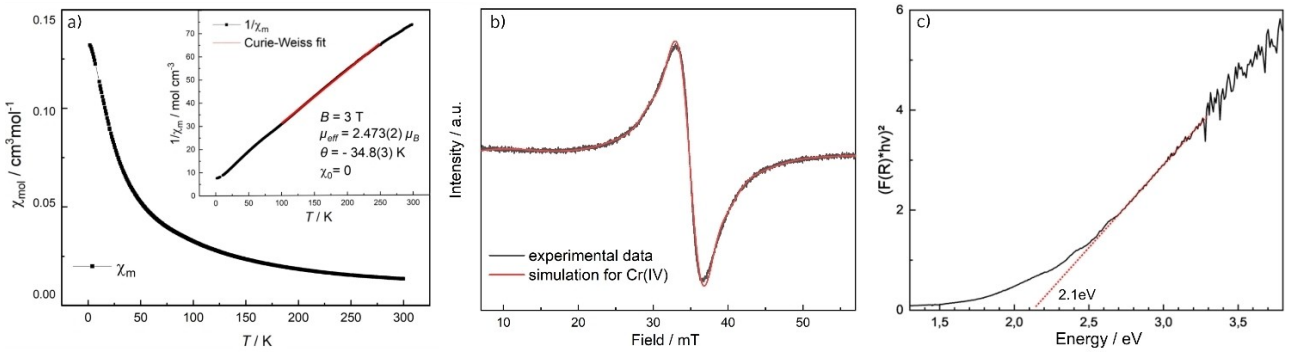

Figure 4. **a)** Magnetic susceptibility of $Cr_{5.7}Si_{2.3}P_8N_{24}$ and inverse magnetic susceptibility (inset) with an extended Curie–Weiss fit (red); **b)** CW X-band EPR spectrum of $Cr_{5.7}Si_{2.3}P_8N_{24}$ measured at 77 K (black) and simulation (red), using the parameters listed in Table S11; **c)** Tauc plot based on the UV/Vis measurement with an energy axis intercept at 2.1 eV. Absorption data suggest a direct band gap, and linear regression between 2.7 and 3.3 eV was used to determine inflection point yielding the band gap.

ther, the influence of mixed anionic frameworks on the electronic structure and properties like electric conductivity and catalytic behavior can be investigated as replacing the hydroxyl groupwith F, O, or Cl can already be observed in natural amphiboles.

Supporting Information

Deposition number 2324313 contains the supplementary crystallographic data for this paper. These data are provided free of charge by the joint Cambridge Crystallographic Data Centre and Fachinformationszentrum Karlsruhe Access Structures service.

The data that support the findings of this study are available in the Supporting Information of this article. The authors have cited additional references within the Supporting Information.[45–88]

Acknowledgements

Financial support by the Deutsche Forschungsgemeinschaft DFG (projects SCHN 377/18-1 and OE 530/6-1) is gratefully acknowledged. We thank Amalina Buda (Department of Chemistry at LMU Munich) for SEM investigations and the ESRF for beamtime to acquire microfocused single-crystal diffraction data (project CH-6207). Open Access funding enabled and organized by Projekt DEAL.

Conflict of Interest

The authors declare no conflict of interest.

Data Availability Statement

The data that support the findings of this study are available in the supplementary material of this article.

Keywords: amphibole · chromium(+IV) · high-pressure chemistry · nitrides · structure elucidation

[1] F. Liebau, *Structural chemistry of silicates: structure, bonding, and classification*, Springer-Verlag, Berlin Heidelberg **2012**, pp. 59–62.
[2] R. L. Virta, *Asbestos, Kirk-Othmer Encyclopedia of Chemical Technology*, Wiley, Weinheim **2011**, pp 1–40.
[3] L. Eisenburger, P. Strobel, P. J. Schmidt, T. Bräuniger, J. Wright, E. L. Bright, C. Giacobbe, O. Oeckler, W. Schnick, *Angew. Chem. Int. Ed.* **2022**, *61*, e202114902.
[4] S. D. Kloß, W. Schnick, *Angew. Chem. Int. Ed.* **2015**, *54*, 11250–11253.
[5] L. Eisenburger, V. Weippert, C. Paulmann, D. Johrendt, O. Oeckler, W. Schnick, *Angew. Chem. Int. Ed.* **2022**, *61*, e202202014.
[6] L. Eisenburger, O. Oeckler, W. Schnick, *Chem. Eur. J.* **2021**, *27*, 4461–4465.
[7] L. Eisenburger, V. Weippert, O. Oeckler, W. Schnick, *Chem. Eur. J.* **2021**, *27*, 14184–14188.
[8] L. Neudert, F. Heinke, T. Bräuniger, F. J. Pucher, G. B. Vaughan, O. Oeckler, W. Schnick, *Chem. Commun.* **2017**, *53*, 2709–2712.
[9] R. D. Shannon, *Acta Crystallogr. Sect. A* **1976**, *32*, 751–767.
[10] S. Pennycook, *Annu. Rev. Mater. Sci.* **1992**, *22*, 171–195.
[11] T. Yong, P. Dera, D. Zhang, *Phys. Chem. Miner.* **2019**, *46*, 215–227.
[12] R. Oberti, G. Della Ventura, F. Cámara, *Rev. Mineral. Geochem.* **2007**, *67*, 89–124.
[13] M. Schwarz, G. Miehe, A. Zerr, E. Kroke, B. T. Poe, H. Fuess, R. Riedel, *Adv. Mater.* **2000**, *12*, 883–887.
[14] S. Vogel, A. T. Buda, W. Schnick, *Angew. Chem. Int. Ed.* **2019**, *131*, 3436–3439.
[15] M. Nardin, C. Lorthioir, M. M. Barberon, R. Madar, E. Fruchart, R. Fruchart, *C. R. Seances Acad. Sci. Ser. C* **1972**, *274*, 2168–2171.
[16] C. Samson, J.-P. Bouchaud, R. Fruchart, *C. R. Seances Acad. Sci. Ser. C* **1964**, *259*, 392–393.
[17] H. Boller, *Monatsh. Chem.* **1968**, *99*, 2444–2449.
[18] H. Boller, *Monatsh. Chem.* **1969**, *100*, 1471–1476.
[19] R. Blix, *Z. Phys. Chem. Abt. B* **1929**, *3*, 229–239.
[20] M. I. Aivazov, T. V. Rezchikova, V. F. Degtyareva, *Inorg. Mater.* **1975**, *11*, 201–203.
[21] R. Kieffer, P. Ettmayer, F. Petter, *Monatsh. Chem.* **1971**, *102*, 1182–1196.
[22] D. A. Vennos, M. E. Badding, F. J. DiSalvo, *Inorg. Chem.* **1990**, *29*, 4059–4062.
[23] M. G. Barker, M. J. Begley, P. P. Edwards, D. H. Gregory, S. E. Smith, *J. Chem. Soc. Dalton Trans.* **1996**, *1*, 1–5.
[24] P. Chanhom, K. E. Fritz, L. A. Burton, J. Kloppenburg, Y. Filinchuk, A. Senyshyn, M. Wang, Z. Feng, N. Insin, J. Suntivich, G. Hautier, *J. Am. Chem. Soc.* **2019**, *141*, 10595–10598.
[25] N. Gloriozova, Y. Prots, F. Jach, M. Krnel, M. Bobnar, A. Ormeci, Y. Grin, P. Höhn, *Inorg. Chem.* **2023**, *62*, 12940–12946.
[26] F. Chevire, C. Ranjan, F. J. DiSalvo, *Solid State Commun.* **2009**, *149*, 273–276.
[27] A. Tennstedt, R. Kniep, M. Hueber, W. Haase, *Z. Anorg. Allg. Chem.* **1995**, *621*, 511–515.
[28] O. Hochrein, M. Kohout, W. Schnelle, R. Kniep, *Z. Anorg. Allg. Chem.* **2002**, *628*, 2738–2743.
[29] R. Juza, J. Haug, *Z. Anorg. Allg. Chem.* **1961**, *309*, 276–282.
[30] A. Gudat, S. Haag, R. Kniep, A. Rabenau, *Z. Naturforsch. B* **1990**, *45*, 111–120.
[31] R. Niewa, D. A. Zherebtsov, P. Hoehn, *Z. Kristallogr. New Cryst. Struct.* **2003**, *218*, 163.
[32] J. R. Akridge, J. H. Kennedy, *J. Solid State Chem.* **1978**, *26*, 147–152.
[33] K. Motizuki, H. Ido, T. Itoh, M. Morifuji, *Electronic Structure and Magnetism of 3d-Transition Metal Pnictides*, Springer Series in Materials Science, Springer-Verlag, Berlin **2010**, pp. 17–71.
[34] M. Yang, A. Zakutayev, J. Vidal, X. Zhang, D. S. Ginley, F. J. DiSalvo, *Energy Environ. Sci.* **2013**, *6*, 2994–2999.
[35] A. Zakutayev, A. J. Allen, X. Zhang, J. Vidal, Z. Cui, S. Lany, M. Yang, F. J. DiSalvo, D. S. Ginley, *Chem. Mater.* **2014**, *26*, 4970–4977.
[36] N. Feldberg, J. Aldous, W. Linhart, L. Phillips, K. Durose, P. Stampe, R. Kennedy, D. Scanlon, G. Vardar, R. Field, *Appl. Phys. Lett.* **2013**, *103*, 042109.
[37] T. Veal, N. Feldberg, N. F. Quackenbush, W. M. Linhart, D. O. Scanlon, L. F. Piper, S. M. Durbin, *Adv. Energy Mater.* **2015**, *5*, 1501462.
[38] J. M. Morbec, I. Narkeviciute, T. F. Jaramillo, G. Galli, *Phys. Rev. B* **2014**, *90*, 155204.

[39] T. Tansley, C. Foley, *J. Appl. Phys.* **1986**, *59*, 3241–3244.
[40] R. S. Ningthoujam, N. S. Gajbhiye, *Prog. Mater. Sci.* **2015**, *70*, 50–154.
[41] X. Meng, W. Qi, W. Kuang, S. Adimi, H. Guo, T. Thomas, S. Liu, Z. Wang, M. Yang, *J. Mater. Chem. A* **2020**, *8*, 15774–15781.
[42] P. Eklund, S. Kerdsongpanya, B. Alling, *J. Mater. Chem. C* **2016**, *4*, 3905–3914.
[43] E. Schmidbauer, T. Kunzmann, T. Fehr, R. Hochleitner, *Phys. Chem. Miner.* **1996**, *23*, 99–106.
[44] D. Wang, Y. Gui, Y. Yu, S. Karato, *Contrib. Mineral. Petrol.* **2012**, *164*, 17–25.
[45] A. Stock, H. Grüneberg, *Ber. Dtsch. Chem. Ges.* **1907**, *40*, 2573–2578.
[46] W. J. Frierson, W. F. Filbert, *Inorg. Synth.*, Wiley-Blackwell, Hoboken, New Jersey **2007**, pp. 136–138.
[47] D. Rubie, *Phase Transitions* **1999**, *68*, 431–451.
[48] D. Walker, *Am. Mineral.* **1991**, *76*, 1092–1100.
[49] D. Walker, M. Carpenter, C. Hitch, *Am. Mineral.* **1990**, *75*, 1020–1028.
[50] H. Huppertz, *Z. Kristallogr.—Cryst. Mater.* **2004**, *219*, 330–338.
[51] H. M. Rietveld, *J. Appl. Crystallogr.* **1969**, *2*, 65–71.
[52] A. Coelho, TOPAS Academic, version 6.1 **2007**.
[53] J. Wright, C. Giacobbe, M. Majkut, *Curr. Opin. Solid State Mater. Sci.* **2020**, *24*, 100818.
[54] CrysAlis^{PRO}, Rigaku Oxford Diffraction Ltd, Yarnton, Oxfordshire **2017**.
[55] G. M. Sheldrick, *Acta Crystallogr. Sect. C* **2015**, *71*, 3–8.
[56] C. B. Hübschle, G. M. Sheldrick, B. Dittrich, *J. Appl. Crystallogr.* **2011**, *44*, 1281–1284.
[57] A. S. Wills, *VaList*, University College London, London **1998–2010**.
[58] N. E. Brese, M. O'Keeffe, *Acta Crystallogr. Sect. B* **1991**, *47*, 192–197.
[59] R. Hoppe, *Angew. Chem. Int. Ed. Engl.* **1970**, *9*, 25–34.
[60] R. Hoppe, *Angew. Chem. Int. Ed. Engl.* **1966**, *5*, 95–106.
[61] DigitalMicrograph, Gatan, Pleasanton, California **1999**.
[62] J. L. Lábár, *Ultramicroscopy* **2005**, *103*, 237–249.
[63] P. A. Stadelmann, *Ultramicroscopy* **1987**, *21*, 131–145.
[64] Velox, version 3, Thermo Fisher Scientific, Waltham, Massachusetts **2021**.
[65] PPMS MultiVu, version 1.5.11 ed., Quantum Design Inc., San Diego, California **2013**.
[66] S. Stoll, A. Schweiger, *J. Magn. Reson.* **2006**, *178*, 42–55.
[67] J. Tauc, R. Grigorovici, A. Vancu, *Phys. Status Solidi B* **1966**, *15*, 627–637.
[68] K. Landskron, PhD thesis, Ludwig-Maximilians-Universität (DE) **2001**.
[69] K. Köllisch, PhD thesis, Ludwig-Maximilians-Universität (DE) **2001**.
[70] H. D. Grundy, F. C. Hawthorne, *Can. Mineral.* **1976**, *14*, 334–345.
[71] R. Oberti, F. Camara, J. M. Caballero, *Am. Mineral.* **2004**, *89*, 888–893.
[72] R. Oberti, F. C. Hawthorne, F. Camara, M. Raudsepp, *Am. Mineral.* **1999**, *84*, 102–111.
[73] M. D. Welch, J. J. Reece, S. A. T. Redfern, *Mineral. Mag.* **2008**, *72*, 877–886.
[74] G. D. Ventura, J. L. Robert, M. Raudsepp, F. C. Hawthorne, M. D. Welch, *Am. Mineral.* **1997**, *82*, 291–301.
[75] R. Oberti, M. Boiocchi, F. C. Hawthorne, R. Kristiansen, *Mineral. Mag.* **2014**, *78*, 861–869.
[76] A. Reitz, H. Pazniak, C. Shen, H. K. Singh, K. Jayanthi, N. Kubitza, A. Navrotsky, H. Zhang, U. Wiedwald, C. S. Birkel, *Chem. Mater.* **2022**, *34*, 10304–10310.
[77] L. Zu, B. Hong, S. Lin, M. Yang, Z. Wang, Y. Zhang, W. Zhao, *J. Alloys Compd.* **2023**, *939*, 168681.
[78] P. Ettmayer, A. Vendl, G. Banik, R. Kieffer, *Monatsh. Chem.* **1978**, *109*, 1005–1008.
[79] S.-J. Kim, T. Marquart, H. F. Franzen, *J. Less-Common Met.* **1990**, *158*, 9–10.
[80] R. Marchand, V. Lemarchand, *J. Less-Common Met.* **1981**, *80*, 157–163.
[81] S. Broll, W. Jeitschko, *Z. Naturforsch. B* **1995**, *50*, 905–912.
[82] K. S. Weil, P. N. Kumt, *J. Solid State Chem.* **1997**, *128*, 185–190.
[83] T. Steiner, S. R. Meka, B. Rheingans, E. Bischof, T. Waldenmaier, G. Yeli, T. L. Martina, P. A. J. Bagot, M. P. Moody, E. J. Mittemeijer, *Philos. Mag.* **2016**, *96*, 1509–1537.
[84] R. Benz, W. H. Zachariasen, *J. Nucl. Mater.* **1970**, *37*, 109–113.
[85] M. S. Bailey, M. N. Obrovac, E. Baillet, T. K. Reynolds, D. B. Zax, F. J. DiSalvo, *Inorg. Chem.* **2003**, *42*, 5572–5578.
[86] M. S. Bailey, F. J. DiSalvo, *Dalton Trans.* **2003**, 2621–2625.
[87] N. W. Falb, J. N. Neu, T. Besara, J. B. Whalen, D. J. Singh, T. Siegrist, *Inorg. Chem.* **2019**, *58*, 3302–3307.
[88] Y. Cao, M. A. Kirsanova, M. Ochi, W. Al Maksoud, T. Zhu, R. Rai, S. Gao, T. Tsumori, S. Kobayashi, S. Kawaguchi, E. Abou-Hamad, K. Kuroki, C. Tassel, A. M. Abakumov, Y. Kobayashi, H. Kageyama, *Angew. Chem. Int. Ed.* **2022**, *61*, e202209187.

Manuscript received: January 20, 2024
Accepted manuscript online: February 15, 2024
Version of record online: March 4, 2024